Published in final edited form as:
Bioconjug Chem. 2010 August 18; 21(8): 1486–1493. doi:10.1021/bc100095w.

Glycan Encapsulated Gold Nanoparticles Selectively Inhibit Shiga Toxins 1 and 2

Ashish A. Kulkarni[†], **Cynthia Fuller-Schaefer**[‡], **Henry Korman**[†], **Alison A. Weiss**[‡,*], and **Suri S. Iyer**[†,*]

[†] UC Chemical and Biosensors group, Department of Chemistry, University of Cincinnati, Cincinnati, Ohio. 45221-0172

[‡] Department of Biochemistry, Molecular Genetics and Microbiology, University of Cincinnati, Cincinnati, Ohio. 45267-0524

Abstract

Shiga toxins (Stx) released by *Escherichia coli* O157:H7 and *Shigella dysentriae*, cause life-threatening conditions that include hemolytic-uremic syndrome (HUS), kidney failure and neurological complications. Cellular entry is mediated by the B subunit of the AB5 toxin, which recognizes cell surface glycolipids present in lipid raft like structures. We developed gold glyconanoparticles that present a multivalent display similar to the cell surface glycolipids to compete for these toxins. These highly soluble glyconanoparticles were nontoxic to the Vero monkey kidney cell line and protected Vero cells from Stx-mediated toxicity in a dose dependent manner. The inhibition is highly dependent on the structure and density of the glycans; selective inhibition of Stx1 and the more clinically relevant Stx2 was achieved. Interestingly, natural variants of Stx2, Stx2c and Stx2d, possessing minimal amino acid variation in the receptor binding site of the B subunit or changes in the A subunit were not neutralized by either the Stx1- or Stx2-specific gold glyconanoparticles. Our results suggest that tailored glyconanoparticles that mimic the natural display of glycans in lipid rafts could serve as potential therapeutics for Stx1 and Stx2. However, a few amino acid changes in emerging Stx2 variants can change receptor specificity, and further research is needed to develop receptor mimics for the emerging variants of Stx2.

INTRODUCTION

Shiga toxin (Stx) is the major pathogenic determinant of several Gram negative bacteria including *Escherichia coli* O157:H7 and *Shigella dysentriae*. Of the estimated 70,000 *E. coli* O157:H7 cases of disease per year in the United States, 10–15% develop hemolytic uremic syndrome (HUS); 3–5% succumb during the acute phase of the disease; and an equivalent number suffer brain damage and renal failure.(1) Treatment of this disease is mostly supportive as postdiarrheal antibiotic treatment enhances toxin production and progression towards HUS.(2) Therefore, there is a great need to develop competitive inhibitors as prophylactics or therapeutics for this untreatable disease.

Stx is a member of the AB_5 family of toxins. There are two major antigenic forms, Stx1 and Stx2, of which Stx2 is more potent than Stx1.(3) The A subunit exhibits RNA N-glycosidase

alison.weiss@uc.edu ; suri.iyer@uc.edu, Fax: 1 513 556 9239.

SUPPORTING INFORMATION AVAILABLE

Detailed procedures of the synthesis of the GNPs and characterization data are given in the supporting material. Additionally, the TEM pictures, and NMR and IR spectra for the GNPs are provided. This material is available free of charge via the Internet at http://pubs.acs.org.

catalytic activity and cleaves a single adenine base from the host cell 28S ribosomal RNA, rendering the ribosome incapable of protein synthesis, leading to cell death. The B, or binding, subunit is a homopentamer with pentaradial symmetry that binds to globotriaosylceramide (Gb3, Figure 1A) in lipid rafts on the cell surface and ultimately delivers the A subunit to its cytoplasmic target.(4) Several designer ligands bearing multiple copies of carbohydrate portion (Pk trisaccharide) of Gb3 to neutralize the action of Stx have been synthesized. Some of these constructs have been demonstrated to possess subnanomolar binding affinities and inhibit the toxins in animal models.(5–9) Unfortunately, phase I human clinical trials using some of these novel compounds were not very promising.(10) A possible reason could be that Stx1, the less potent toxin, and not the more potent clinically significant variant Stx2, was neutralized by these tailored glycoconjugates. Epidemiological studies indicate that *E.coli* O157:H7 infections that lead to the life threatening HUS are mainly associated with strains that produce Stx2 and not Stx1.(11) Primate and murine models of disease indicate that Stx2 is more potent than Stx1.(3,12) In addition, the two forms of toxin display very different tissue localization preferences one hour and 24 hours post injection in mice.(3,13) These results suggest that while both Stx1 and Stx2 display a gross affinity for Gb3, they also recognize fine differences in glycan display associated with different organ systems, and these differences in receptor recognition likely influence toxin potency. Despite the differences in potency between the two toxins, development of therapeutics for both variants is ideal because strains of bacteria can produce both toxins. Additionally, since genes for the toxins can be readily exchanged, commensal bacteria can also produce the variants.(14) Indeed, the CDC recommends testing for the toxin variants and not just *E.coli* O157:H7. (15)

Using an ELISA platform, we recently identified novel ligands that bind specifically to Stx2 with high affinity and not to Stx1.(16) The major difference between these ligands and Pk trisaccharide is the presence of N-acetyl groups at the 2 position of the galactose moiety. (Figure 1B).(17) Based on these discoveries, we developed nanoparticles as potential therapies to inhibit both variants.

We used noble metal nanoparticles to obtain a multivalent display as these nanoparticles are increasingly being used for a variety of applications that include cancer imaging,(18,19) self assembled nano/microstructures,(20,21) targeted delivery (22,23) and anti-adhesives.(24) Glycan encapsulated gold nanoparticles (GNP) are excellent biomaterials as they offer a multivalent display of glycans similar to the glycocalyx structures covering the surface of cells. Additionally, these materials offer several advantages that include water solubility, ease of preparation, stability, cost and absence of toxicity.(25–27) GNPs have been used for the detection of lectins(28) and toxins,(29,30) capture of *E.coli*,(30) pre-symptomatic imaging of brain disease (31) and the inhibition of melanoma cells to the endothelium.(32) GNPs have also been used to examine weak glycan-glycan interactions.(33–35) While examples of small molecule encapsulated nanoparticle as anti-adhesives to competitively inhibit HIV, (36,37) monkey pox (38) and hepatitis B viruses(39) have been reported, GNPs for the inhibition of toxins and pathogens are limited despite the significant advantages offered by these biomaterials.

In this study, we developed different analogues of Pk trisaccharide, the glycan that exhibits preferential binding to Stx (Figure 1A), and coated them onto gold nanoparticles. Next, we assessed the ability of GNPs coated with Pk trisaccharide analogues to neutralize Stx in a protein-synthesis inhibition assay. We found that these GNPs are excellent inhibitors of two variants of Stx. We also found that inhibition is highly dependent on the structure and density of the glycan and additionally, the structure of the toxin.

EXPERIMENTAL PROCEDURES

Materials

All chemical reagents were of analytical grade, used as supplied without further purification unless indicated. Acetic anhydride and acetyl chloride were distilled under an inert atmosphere and stored under argon. 4Å Molecular sieves were stored in an oven (>130 ºC) and cooled in vacuo. The acidic ion-exchange resin used was Dowex-50 and Amberlite (H+ form). Analytical thin layer chromatography (TLC) was conducted on silica gel 60-F254 (Merck). Plates were visualized under UV light, and/or by treatment with acidic cerium ammonium molybdate followed by heating. Column chromatography was conducted using silica gel (230–400 mesh) from Qualigens. 1H and 13C NMR spectra were recorded on Bruker AMX 400MHz spectrometer. Chemical shifts are reported in δ (ppm) units using 13C and residual 1H signals from deuterated solvents as references. Spectra were analyzed with Mest-Re-C Lite (Mestrelab Research) and/or XWinPlot (Bruker Biospin). Electrospray ionization mass spectra were recorded on a Micromass Q Tof 2 (Waters) and data were analyzed with MassLynx 4.0 (Waters) software.

Synthesis of GNPs

The synthesis and complete characterization of the glycans and intermediates are given in the supporting information. Using these glycans, GNPs were synthesized using the *in situ* procedure.(40, 41) A representative example is described. Briefly, 0.25 ml of a 1% $HAuCl_4$ solution was added to 50 ml of deionized H_2O. Next, LG1 (2.35 mg, 0.0018 mmol) or LG2 (2.5 mg, 0.0018 mmol) was added. To this solution, previously cooled $NaBH_4$ solution (0.16 ml, 0.5 mg/ml) was added dropwise with rapid stirring at 0°C. The color of the solution changed from light yellow to brown. The resulting brownish solution was stirred for an additional 2h. The solvent was evaporated *in vacuo* and the resulting brownish residue was suspended in 100 ml of CH_3OH and sonicated for 10 min. The resulting slurry was centrifuged at 5000 *g* for 1h to precipitate the GNPs. The supernatant was removed and this procedure was repeated three times to remove the excess glycan. The GNPs were dissolved in 1 ml deionized H_2O and lyophilized to yield 1 mg of pure GNPs.

TEM measurements

The TEM analysis were obtained on a Philips CM20 machine. Briefly, 1 μl of a suspension of the nanoparticle (10 μg dissolved in 1 ml of deionized water) was placed on a copper grid (200 mesh carbon coated) and the sample was evaporated overnight. A minimum of 50 GNPs were measured to obtain the mean particle diameter and standard deviation. (Supporting Information)

Determination of number of carbohdyrates per nanoparticle

The number of carbohydrates was determined by anthrone-sulfuric acid assay. (41) Briefly, carbohydrates (1 to 15 μg) were dissolved in 0.5 ml of deionized water. Next, 1 ml of a freshly prepared solution of 0.5% anthrone (w/w) in 95% sulfuric acid was added to 0.5 ml of ice cold sugar solution. The resulting solution was gently mixed and heated to 100°C for 10 min and the allowed to cool to RT. The absorbance was recorded at 620 nm and the plot of absorbance versus concentration of carbohydrate resulted in a standard curve. Next, different concentrations of the GNPs (100–500 μg) were subjected to the same method. From this concentration, the concentration of sugars in 1mg of NPs was obtained and the number of carbohydrates per nanoparticle was calculated. (Supporting Information)

Protein inhibition assay

Vero cells expressing destabilized luciferase (*luc2P* Vero cells) were obtained as follows. The gene for destabilized luciferase, *luc2P*, was excised from pGL4.11[luc2p] (Promega, Madison, WI) with *Hin*dIII and *Xba*I, blunted using Klenow, and cloned into the *Hpa*I site of MigR1.(42) HEK GP2-293 retrovirus packaging strain (Clontech, Mountain View, CA) was incubated with 3 μg Luc2p-MigR1 DNA and 1 μg pVSV-G envelope as previously described.(43) Transfected Vero cells were sorted by flow cytometry, GFP positive cells were propagated, and sorted a second time to obtain cells expressing high levels of GFP.(44) These cells have been deposited with the Biodefense and Emerging Infections Research Resources Repository http://www.beiresources.org/. Crude or purified toxins were diluted in phosphate buffered saline (PBS), followed by half-log serial dilutions; 25μl of each dilution was added to white tissue culture-treated, Falcon 96-well microtiter plates (Becton Dickinson, Franklin Lakes, NJ). 100 μl containing 10^4 luciferase-expressing Vero cells was added to the wells and the plates were incubated for 4 hours at 37ºC with 5% CO_2. The cells were washed three times with PBS, 25μl Superlite Luciferase Substrate (Bioassay Systems, Hayward, CA) was added, and light was measured using the Luminoskan *Ascent* (Thermo Labsystems, Helsinki, Finland). *luc2P* Vero cells incubated without toxin were used as the negative control to determine maximum light production (maximum protein synthesis). The Effective Dose (ED_{50}; amount of toxin required to achieve a 50% reduction in protein synthesis) was calculated using the two points above and below the mid-point.

Determination of surface density of glycans on nanoparticle surface

The distance between glycans were calculated as described previously with slight modifications.(45) Briefly, the following assumptions were made. (i) The nanoparticles were considered as spheres of 4 nm diameter. (ii) Glycans were assumed to be equally distributed on the nanoparticle surface. (iii) Glycans were assumed to be situated perpendicular to the surface and parallel to each other.

Average surface area of the nanoparticle was determined by using formula $4\pi r^2$, where r is radius of nanoparticle, 2 nm. Since we know the average number of glycans on the nanoparticle surface, we can calculate the average surface density by taking ratio of number of glycans over surface density. So, average surface density is 1.3 glycans per nm^2. In order to calculate the distance between two glycans, we assumed that there are average 1.3 glycans in a square of 1nm side. Average distance between two glycans can be approximated by using formula ($\sqrt{A}/n$), where A is area of the square which is 1 nm^2 and n is number of glycans.

RESULTS AND DISCUSSION

Synthesis of gold glyconanoparticles (GNP)

Using our previously published synthetic strategy, we synthesized Pk trisaccharide analogues (Scheme 1 and 2, Supporting Information) with linkers terminated with thiol groups (Figure 1B, LG1 and LG2). Thiolated ligands were used as they can readily be attached to gold nanoparticles. A thiolated β galactoside derivative was synthesized as a negative control (Figure 1B, LG3). Next, GNPs were synthesized by previously published method (40, 41) to yield uniform spherical nanoparticles of narrow size distribution (~ 4 nm). These GNPs were characterized using NMR, UV, IR and TEM spectroscopies (Supporting Information). The number of glycans conjugated on the nanoparticle surface was determined by using the anthrone method.(41) (Table 1, Supporting Information) We also synthesized GNP's with different surface densities of glycans by premixing the glycans with a spectator thiolated oligoethylene glycol ligand (OEG, Figure 1) to study the effect of surface density on binding.

Neutralization of Stx variants using a protein inhibition assay

Stx inhibits protein synthesis by cleaving the 28S ribosomal RNA. We developed a protein inhibition assay (44) to quantify the influence of Stx on protein synthesis in the presence and absence of GNPs (Figure 3A). Vero cells were transfected with the MigR1 lentivirus (42) containing the cloned *luc2P* gene (destabilized luciferase, from pGL4, Promega, Madison, WI), encoding the gene for luciferase fused to the PEST motif (proline-glutamic acid-serine-threonine), which targets the protein for degradation by the proteosome. This construct allows us to directly measure the rate of protein synthesis by measuring bioluminescence generated by luciferase-mediated oxidation of luciferin. We used this assay as opposed to the MTT assay, because the latter suffers from the problem that it only measures metabolic activity (e.g. due to cell death), not protein synthesis inhibition, and thus only indirectly reflects Shiga toxin activity. The luciferase assay directly indicates toxin-mediated inhibition of protein synthesis. Furthermore, the MTT assay requires 3 days compared to 4 hours for the luciferase assay. We evaluated the cytotoxicity of GNPs towards *luc2P* Vero cells by comparing the cells incubated with GNPs to the PBS buffer control. As shown in Figure 2, protein synthesis was unaltered in presence of GNPs, indicating that the GNPs are not cytotoxic to *luc2P* Vero cells.

Next, we studied the ability of the GNPs to neutralize Stx (Figure 3A). Briefly, serial dilutions of Stx ranging from 0.01 to 64 ng were added to the wells of 96-well microtiter plates. GNPs were added at 10μg/well to the wells and allowed to incubate for 15 minutes, followed by the addition of 10^4 cells/well. (Please see *Experimental procedures* section) Plates were incubated at 37°C in 5% CO_2 for 4 hours. The cells were washed with PBS, followed by addition of 100 μl/well of SuperLight™ Luciferase substrate solution (BioAssay Systems; Hayward, CA) containing luciferin, and luminescence was measured using a luminometer (Thermo Labsystems Luminoskan Ascent; Helsinki, Finland) and reported as percentage of maximum signal (% no toxin control). Results for Stx1 are shown in Figure 3B. The blue line indicates the amount of protein synthesis in the presence of different concentrations of Stx1. When we incubated Stx1 with GNP1 (which has Pk saccharide on the nanoparticle surface) prior to addition of cells, we observed significant protection of Vero cells (red line). In contrast, GNP3, β-galactoside coated nanoparticles (violet line) failed to protect the Vero cells from Stx1 while GNP2, which has the N-acetylated version of Pk saccharide on the surface of the nanoparticles (green line) afforded minimal protection, indicating selective inhibition by the GNPs.

Selective neutralization of Stx2 was also observed (Figure 3C). GNP2, the nanoparticle coated with LG2, afforded significant protection of Vero cells from Stx2, (green line) whereas GNP1 exhibited minimal protection of cells from this variant. As in the case of Stx1, β-galactoside coated nanoparticles did not protect cells from Stx2. Preliminary studies using culture supernatant supported previous studies demonstrating that NHAc-Pk GNP2 was not effective at neutralizing Stx1 and Pk GNP1 was not effective at neutralizing Stx2 (Table 1). These studies emphasize the importance of using the appropriate ligand to inhibit the specific variant as small changes in the structure of the glycan can impact the inhibitory activity significantly.

The ED_{50} (Effective Dose that produces 50% response) values for purifed Stx1 and Stx2 with the different GNPs (100 μg/mL) are given in Table 1. The ED_{50} of purified Stx1 was 0.07 ng/ml with Vero cells without any inhibitor. When Stx1 was preincubated with GNP1, the ED_{50} value increased to 25.6 ng/ml, demonstrating 366 times more toxin is needed to inhibit 50% protein synthesis in presence of GNP1 compared to toxin alone. In the case of Stx2, the ED_{50} of Stx2 was 0.6 ng/ml with Vero cells without any inhibitor. When Stx2 was preincubated with GNP2, an ED_{50} value of 92 ng/ml was obtained, or 153 times more toxin was needed to inhibit 50% protein synthesis in presence of GNP2 than toxin alone. In vitro,

neutralization with the GNPs occurred at a ratio of about 80 GNPs per Stx2 molecule, or about 5,000 glycans per toxin molecule. While we have not investigated neutralization *in vivo*, *in vivo* studies using Starfish and Daisy inhibitors observed neutralization at ratios of 1,000 to 10,000 inhibitor molecules per toxin molecule.(5,9)

Next, we investigated the ability of the GNP's to inhibit emerging variants of Stx2, Stx2c and Stx2d. The amino acid sequence for these variants is shown in Figure 4A. The B-subunit of Stx2c differs from Stx2 by two amino acids (D16N, D24A), of which position 16 is present in the predicted receptor binding site. These differences lead to a significant drop in the ED_{50} of Stx2c (61ng/ml) compared to Stx2 (0.6ng/ml) with cells alone. Since there are five B subunits in each variant, which binds to a minimum of five glycolipids in a multivalent manner, a single mutation in the receptor binding site would have a fivefold effect on the ED_{50}. (Figure 4A and B) When Stx2c is preincubated with either of the GNPs and exposed to Vero cells, minimal 2-fold protection was observed, which was not statistically significant. (Table 1) The lack of neutralization could be due to the inherently decreased toxicity of Stx2c. Alternatively, the amino acid changes could alter the requirements for presentation of the ligand or its density on the nanoparticle, as orientation effects have been demonstrated to influence binding.(46, 47)

The ED_{50} of Stx2d (0.5 ng/ml) is very similar to that of Stx2 (0.6 ng/ml). However, we observed minimal protection with either GNP. The B-subunit of Stx2d differs from Stx2 by only one amino acid, which is not thought to be in a receptor binding site (I51V, Figure 4A and C). However, the terminal amino acid of the Stx2d A subunit is different from Stx2 in that the basic amino acid, lysine, has been changed to the acidic amino acid, glutamic acid. The amino acids surrounding the central region of the B-pentamer that forms the pore for the A-subunit serves as a glycan binding site in Stx1. It is unclear if this region also serves as a glycan binding site for Stx2, since the C-terminus of Stx2 extends past the B-pentamer pore, which could occlude a binding site, alternatively the A subunit could participate in binding. The different neutralization patterns between Stx2 and Stx2d could be due to the changes in the A terminus. The importance of the C-terminal tail in influencing potency has been established by studies that have shown that a proteolytically processed form of Stx2d (Stx2d*) with last two amino acids removed, is more potent than Stx2d. The activation of Sx2d to the Stx2d* form has been shown to be mediated *in vivo* by elastase present in mucus secretions.(48) Overall, these results demonstrate that minor changes in the structure of the toxin can dramatically affect both potency and neutralization by receptor mimics.

Effect of ligand density on the neutralization of Stxs

We were interested in evaluating the effect of differential glycan density on the surface of the GNPs, as several reports indicate that density is an important factor in determining binding affinities.(49,50) We premixed the ligand with short oligoethylene glycol spacer terminated in a thiol group (OEG, Figure 1) at different ratios (Glycan: OEG; 100:0 25:75) and coated the GNPs similarly. Mean inhibition activity for Stx1 was decreased by 10 fold and for Stx2 was decreased by 3.5 fold for nanoparticles coated at a ratio of 75:25 and 50:50 as compared to the nanoparticles coated at a ratio of 100:0. (Figure 5A and B) However, no inhibition was observed at a ratio of 25:75. (Figure 5A and B) We attribute this decrease to a failure of the toxin to engage multiple glycans. Briefly, for Stx1 there are three proposed binding sites per B subunit, of which site 2 has been shown to be the most important site. (5,51) Stx2 has been proposed to use sites mapping to the corresponding positions. The average distance between the three possible binding sites per B subunit of Stx2 is ~1.2 nm. The distance between site1-site2 is ~ 1.3 nm, site1-site3 is ~ 1.6 nm and site2-site3 is ~ 0.8 nm. The average distance between binding site 2 of 1 B subunit and adjacent B subunit is ~1.8 nm. (Supplementary information) The average distances between adjacent glycans on the nanoparticle surface for 100%, 75% and 50% coverage was calculated to be ~0.9, ~1.2

and ~1.8 nm, respectively.(45) (Figure 5C) Thus, there are multiple glycans to engage the binding sites on the B subunit for these surface densities. When the surface density was decreased to 25%, the average distance is ~3.6 nm, which is greater than the distance between the binding sites on the toxin. This presumably leads to loss of cooperativity and loss in inhibitory activity.

In summary, we have developed an efficient strategy towards the development of gold glyconanoparticles for the selective inhibition of Stx 1 and 2. These nanoparticles are not toxic to Vero cells and can effectively inhibit Stx variants 1 and 2 from inhibiting protein synthesis in Vero cells. We demonstrate that the inhibition is highly dependent on the structure and density of the glycans and the structure of the toxin. A single amino acid variation in the receptor binding site of the B subunit or changes in the A subunit of the toxin fails to inhibit infection. Our results suggest that tailored glyconanoparticles can serve as potential therapeutics for Stx1 and 2, however, further research is needed to develop strain specific or broad spectrum therapeutics for emerging variants.

Supplementary Material

Refer to Web version on PubMed Central for supplementary material.

Acknowledgments

We thank NIAID (U01-AI075498 A.A.W. and S.S.I.) and NSF (Career CHE-0845005 S.S.I.) for providing financial support.

References

1. Siegler RL. Postdiarrheal Shiga toxin-mediated hemolytic uremic syndrome. JAMA. 2003; 290:1379–81. [PubMed: 12966132]
2. Wong CS, Jelacic S, Habeeb RL, Watkins SL, Tarr PI. The risk of the hemolytic-uremic syndrome after antibiotic treatment of Escherichia coli O157:H7 infections. N Engl J Med. 2000; 342:1930–6. [PubMed: 10874060]
3. Rutjes NW, Binnington BA, Smith CR, Maloney MD, Lingwood CA. Differential tissue targeting and pathogenesis of verotoxins 1 and 2 in the mouse animal model. Kidney Int. 2002; 62:832–45. [PubMed: 12164865]
4. Sandvig K, van Deurs B. Endocytosis, intracellular transport, and cytotoxic action of Shiga toxin and ricin. Physiol Rev. 1996; 76:949–66. [PubMed: 8874490]
5. Kitov PI, Sadowska JM, Mulvey G, Armstrong GD, Ling H, Pannu NS, Read RJ, Bundle DR. Shiga-like toxins are neutralized by tailored multivalent carbohydrate ligands. Nature. 2000; 403:669–72. [PubMed: 10688205]
6. Neri P, Nagano SI, Yokoyama S, Dohi H, Kobayashi K, Miura T, Inazu T, Sugiyama T, Nishida Y, Mori H. Neutralizing activity of polyvalent Gb3, Gb2 and galacto-trehalose models against Shiga toxins. Microbiol Immunol. 2007; 51:581–92. [PubMed: 17579269]
7. Dohi H, Nishida Y, Mizuno M, Shinkai M, Kobayashi T, Takeda T, Uzawa H, Kobayashi K. Synthesis of an artificial glycoconjugate polymer carrying Pk-antigenic trisaccharide and its potent neutralization activity against Shiga-like toxin. Bioorg Med Chem. 1999; 7:2053–62. [PubMed: 10530955]
8. Kitov PI, Mulvey GL, Griener TP, Lipinski T, Solomon D, Paszkiewicz E, Jacobson JM, Sadowska JM, Suzuki M, Yamamura K, Armstrong GD, Bundle DR. In vivo supramolecular templating enhances the activity of multivalent ligands: a potential therapeutic against the Escherichia coli O157 AB5 toxins. Proc Natl Acad Sci U S A. 2008; 105:16837–42. [PubMed: 18955695]
9. Griener TP, Mulvey GL, Marcato P, Armstrong GD. Differential binding of Shiga toxin 2 to human and murine neutrophils. J Med Microbiol. 2007; 56:1423–30. [PubMed: 17965340]

10. Trachtman H, Cnaan A, Christen E, Gibbs K, Zhao S, Acheson DW, Weiss R, Kaskel FJ, Spitzer A, Hirschman GH. Effect of an oral Shiga toxin-binding agent on diarrhea-associated hemolytic uremic syndrome in children: a randomized controlled trial. Jama. 2003; 290:1337–44. [PubMed: 12966125]

11. Boerlin P, McEwen SA, Boerlin-Petzold F, Wilson JB, Johnson RP, Gyles CL. Associations between virulence factors of Shiga toxin-producing Escherichia coli and disease in humans. J Clin Microbiol. 1999; 37:497–503. [PubMed: 9986802]

12. Siegler RL, Obrig TG, Pysher TJ, Tesh VL, Denkers ND, Taylor FB. Response to Shiga toxin 1 and 2 in a baboon model of hemolytic uremic syndrome. Pediatr Nephrol. 2003; 18:92–6. [PubMed: 12579394]

13. Armstrong GD, Mulvey GL, Marcato P, Griener TP, Kahan MC, Tennent GA, Sabin CA, Chart H, Pepys MB. Human Serum Amyloid P Component Protects against Escherichia coli O157:H7 Shiga Toxin 2 In Vivo: Therapeutic Implications for Hemolytic-Uremic Syndrome. J Infect Dis. 2006; 193:1120–4. [PubMed: 16544252]

14. Gamage SD, Patton AK, Strasser JE, Chalk CL, Weiss AA. Commensal bacteria influence Escherichia coli O157:H7 persistence and Shiga toxin production in the mouse intestine. Infect Immun. 2006; 74:1977–83. [PubMed: 16495578]

15. Atkinson, R.; Johnson, G.; Root, T.; Halse, T.; Wroblewski, D.; Davies, M.; Byrd, A.; Long, L.; Demma, L.; Angulo, F.; Bopp, C.; Gerner-Smidt, P.; Strockbine, N.; Greene, K.; Swaminathan, B.; Griffin, P.; Schaffzin, J.; Goode, B. Morbidity and Mortality Weekly Report. CDC; 2006. p. 1042-1045.

16. Kale RR, McGannon CM, Fuller-Schaefer C, Hatch DM, Flagler MJ, Gamage SD, Weiss AA, Iyer SS. Differentiation between Structurally Homologous Shiga 1 and Shiga 2 Toxins by Using Synthetic Glycoconjugates. Angew Chem Int Ed Engl. 2008; 47:1265–1268. [PubMed: 18172842]

17. Kale RR, McGannon CM, Fuller-Schaefer C, Hatch DM, Flagler MJ, Gamage SD, Weiss AA, Iyer SS. Differentiation between structurally homologous Shiga 1 and Shiga 2 toxins by using synthetic glycoconjugates. Angew Chem Int Ed Engl. 2008; 47:1265–8. [PubMed: 18172842]

18. Mallidi S, Larson T, Tam J, Joshi PP, Karpiouk A, Sokolov K, Emelianov S. Multiwavelength Photoacoustic Imaging and Plasmon Resonance Coupling of Gold Nanoparticles for Selective Detection of Cancer. Nano Lett. 2009

19. Popovtzer R, Agrawal A, Kotov NA, Popovtzer A, Balter J, Carey TE, Kopelman R. Targeted Gold Nanoparticles Enable Molecular CT Imaging of Cancer. Nano Lett. 2008

20. Zhang J, Wang J, Xu X, Zhu H, Wang Z, Yang F, Zhang B, Yang X. A one-dimensional network from the self-assembly of gold nanoparticles by a necklace-like polyelectrolyte template mediated by metallic ion coordination. Nanotechnology. 2009; 20:295603. [PubMed: 19567954]

21. Toster J, Iyer KS, Burtovyy R, Burgess SS, Luzinov IA, Raston CL. Regiospecific assembly of gold nanoparticles around the pores of diatoms: toward three-dimensional nanoarrays. J Am Chem Soc. 2009; 131:8356–7. [PubMed: 19530723]

22. Muthu MS, Singh S. Targeted nanomedicines: effective treatment modalities for cancer, AIDS and brain disorders. Nanomed. 2009; 4:105–18.

23. Hwu JR, Lin YS, Josephrajan T, Hsu MH, Cheng FY, Yeh CS, Su WC, Shieh DB. Targeted Paclitaxel by conjugation to iron oxide and gold nanoparticles. J Am Chem Soc. 2009; 131:66–8. [PubMed: 19072111]

24. Jain J, Arora S, Rajwade J, Khandelwal S, Paknikar KM. Silver nanoparticles in therapeutics: development of an antimicrobial gel formulation for topical use. Mol Pharm. 2009

25. de La Fuente JM, Barrientos AG, Rojas TC, Rojo J, Canada J, Fernandez A, Penades S. Gold Glyconanoparticles as Water-Soluble Polyvalent Models To Study Carbohydrate Interactions This work was supported by the DGICYT (PB96-0820), J.M.F. thanks the MEC for a predoctoral fellowship. A.G.B. thanks CSIC for financial support. We thank Prof. Martin-Lomas for his scientific and financial support. Angew Chem Int Ed Engl. 2001; 40:2257–2261. [PubMed: 11433487]

26. de la Fuente JM, Penades S. Glyconanoparticles: types, synthesis and applications in glycoscience, biomedicine and material science. Biochim Biophys Acta. 2006; 1760:636–51. [PubMed: 16529864]

27. Barrientos AG, de la Fuente JM, Rojas TC, Fernandez A, Penades S. Gold glyconanoparticles: synthetic polyvalent ligands mimicking glycocalyx-like surfaces as tools for glycobiological studies. Chemistry. 2003; 9:1909–21. [PubMed: 12740837]
28. Lin CC, Yeh YC, Yang CY, Chen GF, Chen YC, Wu YC, Chen CC. Quantitative analysis of multivalent interactions of carbohydrate-encapsulated gold nanoparticles with concanavalin A. Chem Commun (Camb). 2003:2920–1. [PubMed: 14680241]
29. Schofield CL, Field RA, Russell DA. Glyconanoparticles for the colorimetric detection of cholera toxin. Anal Chem. 2007; 79:1356–61. [PubMed: 17297934]
30. El-Boubbou K, Gruden C, Huang X. Magnetic glyco-nanoparticles: a unique tool for rapid pathogen detection, decontamination, and strain differentiation. J Am Chem Soc. 2007; 129:13392–3. [PubMed: 17929928]
31. van Kasteren SI, Campbell SJ, Serres S, Anthony DC, Sibson NR, Davis BG. Glyconanoparticles allow pre-symptomatic in vivo imaging of brain disease. Proc Natl Acad Sci U S A. 2009; 106:18–23. [PubMed: 19106304]
32. Rojo J, Diaz V, de la Fuente JM, Segura I, Barrientos AG, Riese HH, Bernad A, Penades S. Gold glyconanoparticles as new tools in antiadhesive therapy. Chembiochem. 2004; 5:291–7. [PubMed: 14997521]
33. Reynolds AJ, Haines AH, Russell DA. Gold glyconanoparticles for mimics and measurement of metal ion-mediated carbohydrate-carbohydrate interactions. Langmuir. 2006; 22:1156–63. [PubMed: 16430279]
34. de la Fuente JM, Penades S. Understanding carbohydrate-carbohydrate interactions by means of glyconanotechnology. Glycoconj J. 2004; 21:149–63. [PubMed: 15483380]
35. de la Fuente JM, Eaton P, Barrientos AG, Menendez M, Penades S. Thermodynamic evidence for Ca2+-mediated self-aggregation of Lewis X gold glyconanoparticles. A model for cell adhesion via carbohydrate-carbohydrate interaction. J Am Chem Soc. 2005; 127:6192–7. [PubMed: 15853323]
36. Bowman MC, Ballard TE, Ackerson CJ, Feldheim DL, Margolis DM, Melander C. Inhibition of HIV fusion with multivalent gold nanoparticles. J Am Chem Soc. 2008; 130:6896–7. [PubMed: 18473457]
37. Martinez-Avila O, Bedoya LM, Marradi M, Clavel C, Alcami J, Penades S. Multivalent manno-glyconanoparticles inhibit DC-SIGN-mediated HIV-1 trans-infection of human T cells. ChemBioChem. 2009; 10:1806–9. [PubMed: 19565596]
38. Rogers JV, Parkinson CV, Choi YW, Speshock JL, Hussain SM. A preliminary assessment of silver nanoparticle inhibition of monkeypox virus plaque formation. Nanoscale Research Letters. 2008; 3:129–133.
39. Lu L, Sun RWY, Chen R, Hui CK, Ho CM, Luk JM, Lau GKK, Che CM. Silver nanoparticles inhibit hepatitis B virus replication. Antiviral Therapy. 2008; 13:253–262. [PubMed: 18505176]
40. Brust M, Bethell JFD, Schiffrin DJ, Kiely C. Synthesis and Reactions of Functionalised Gold Nanoparticles. J Chem Soc, Chem Comm. 1995:1655–1656.
41. Chien YY, Jan MD, Adak AK, Tzeng HC, Lin YP, Chen YJ, Wang KT, Chen CT, Chen CC, Lin CC. Globotriose-functionalized gold nanoparticles as multivalent probes for Shiga-like toxin. Chembiochem. 2008; 9:1100–9. [PubMed: 18398881]
42. Pear WS, Miller JP, Xu L, Pui JC, Soffer B, Quackenbush RC, Pendergast AM, Bronson R, Aster JC, Scott ML, Baltimore D. Efficient and rapid induction of a chronic myelogenous leukemia-like myeloproliferative disease in mice receiving P210 bcr/abl-transduced bone marrow. Blood. 1998; 92:3780–92. [PubMed: 9808572]
43. Sherrill JD, Miller WE. G protein-coupled receptor (GPCR) kinase 2 regulates agonist-independent Gq/11 signaling from the mouse cytomegalovirus GPCR M33. J Biol Chem. 2006; 281:39796–805. [PubMed: 17088245]
44. McGannon CM, Fuller-Schaefer C, Weiss AA. Different classes of antibiotics differentially influence Shiga toxin production. Antimicrob Agents Chemother. 2010 in press. 10.1128/AAC.01783-09
45. Hill HD, Millstone JE, Banholzer MJ, Mirkin CA. The role radius of curvature plays in thiolated oligonucleotide loading on gold nanoparticles. ACS Nano. 2009; 3:418–24. [PubMed: 19236080]

46. Chandrasekaran A, Srinivasan A, Raman R, Viswanathan K, Raguram S, Tumpey TM, Sasisekharan V, Sasisekharan R. Glycan topology determines human adaptation of avian H5N1 virus hemagglutinin. Nat Biotechnol. 2008; 26:107–13. [PubMed: 18176555]

47. Lewallen DM, Siler D, Iyer SS. Factors Affecting Protein-Glycan Specificity: Effect of Spacers and Incubation Time. ChemBioChem. 2009; 10:1486–1489. [PubMed: 19472251]

48. Kokai-Kun JF, Melton-Celsa AR, O'Brien AD. Elastase in intestinal mucus enhances the cytotoxicity of Shiga toxin type 2d. J Biol Chem. 2000; 275:3713–21. [PubMed: 10652371]

49. Dhayal M, Ratner DM. XPS and SPR analysis of glycoarray surface density. Langmuir. 2009; 25:2181–7. [PubMed: 19199748]

50. Lewallen DM, Siler D, Iyer SS. Factors affecting protein-glycan specificity: effect of spacers and incubation time. ChemBioChem. 2009; 10:1486–9. [PubMed: 19472251]

51. Kitov PI, Shimizu H, Homans SW, Bundle DR. Optimization of tether length in nonglycosidically linked bivalent ligands that target sites 2 and 1 of a Shiga-like toxin. J Am Chem Soc. 2003; 125:3284–94. [PubMed: 12630884]

52. Fraser ME, Fujinaga M, Cherney MM, Melton-Celsa AR, Twiddy EM, O'Brien AD, James MN. Structure of shiga toxin type 2 (Stx2) from Escherichia coli O157:H7. J Biol Chem. 2004; 279:27511–7. [PubMed: 15075327]

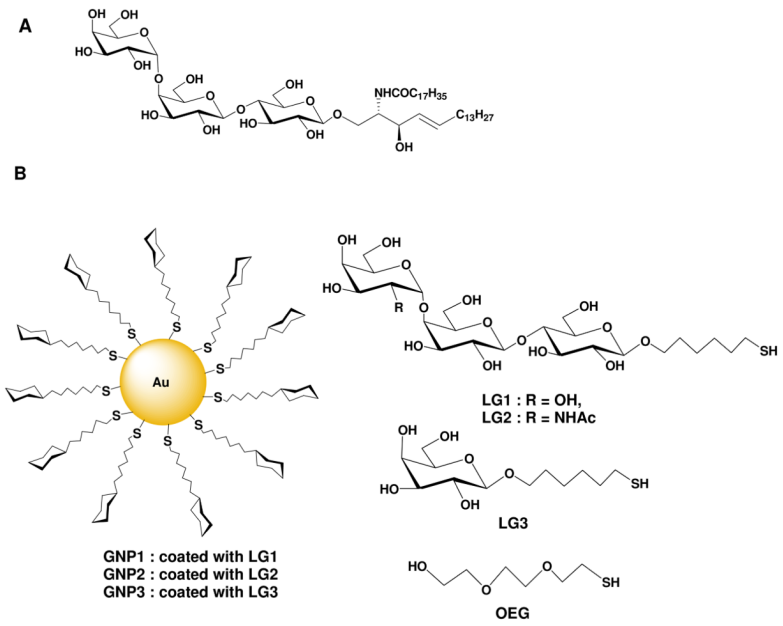

Figure 1.

Relevant glycans. (**A**) Structure of native Gb3. (**B**) Representation of the gold glyconanoparticle and the structures of the three glycans with linkers terminated in thiol.

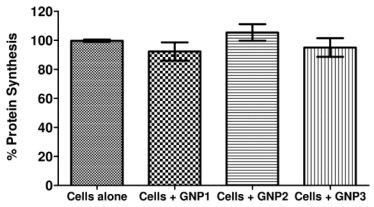

Figure 2.

The effect of GNPs in protein synthesis of *luc2P* Vero cells was evaluated by incubating the cells with 10μg of GNPs or PBS alone. Protein synthesis was unaltered in presence of GNPs indicating that the GNPs do not perturb protein synthesis in *luc2P* Vero cells.

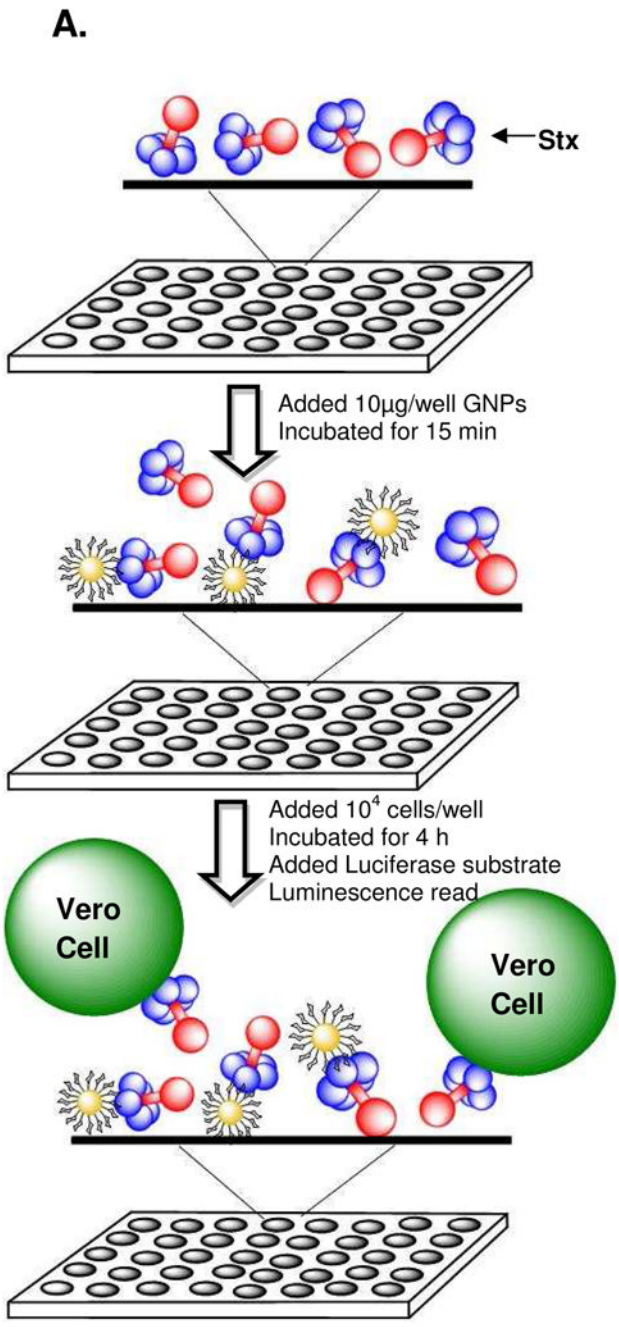

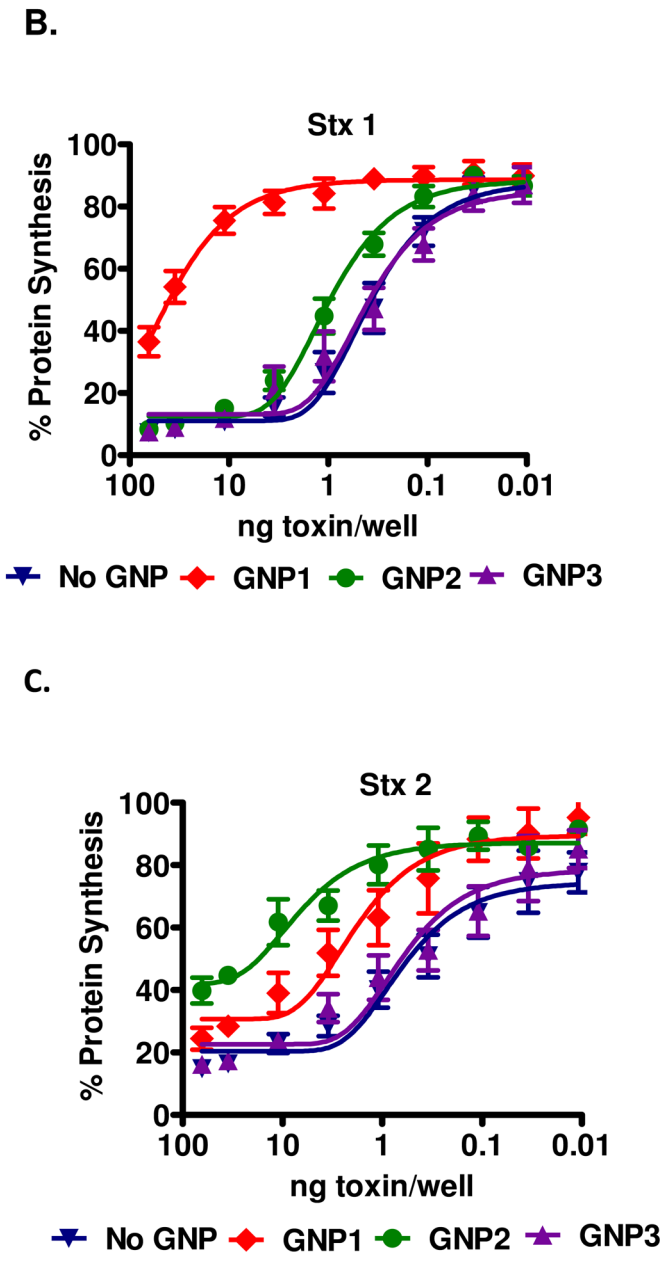

Figure 3.

(**A**) Cartoon presentation of the Vero cell toxin inhibition assay. GNPs were added to wells containing serial dilutions of toxin, followed by addition of 10^4 Vero cells expressing a destabilized form of luciferase, *luc2P*. Plates were incubated at 37°C for 4h. Luciferase substrate was added and luminescence was measured on a luminometer. (**B**) Inhibition of Stx1 using GNPs. (**C**) Inhibition of Stx2 using GNPs.

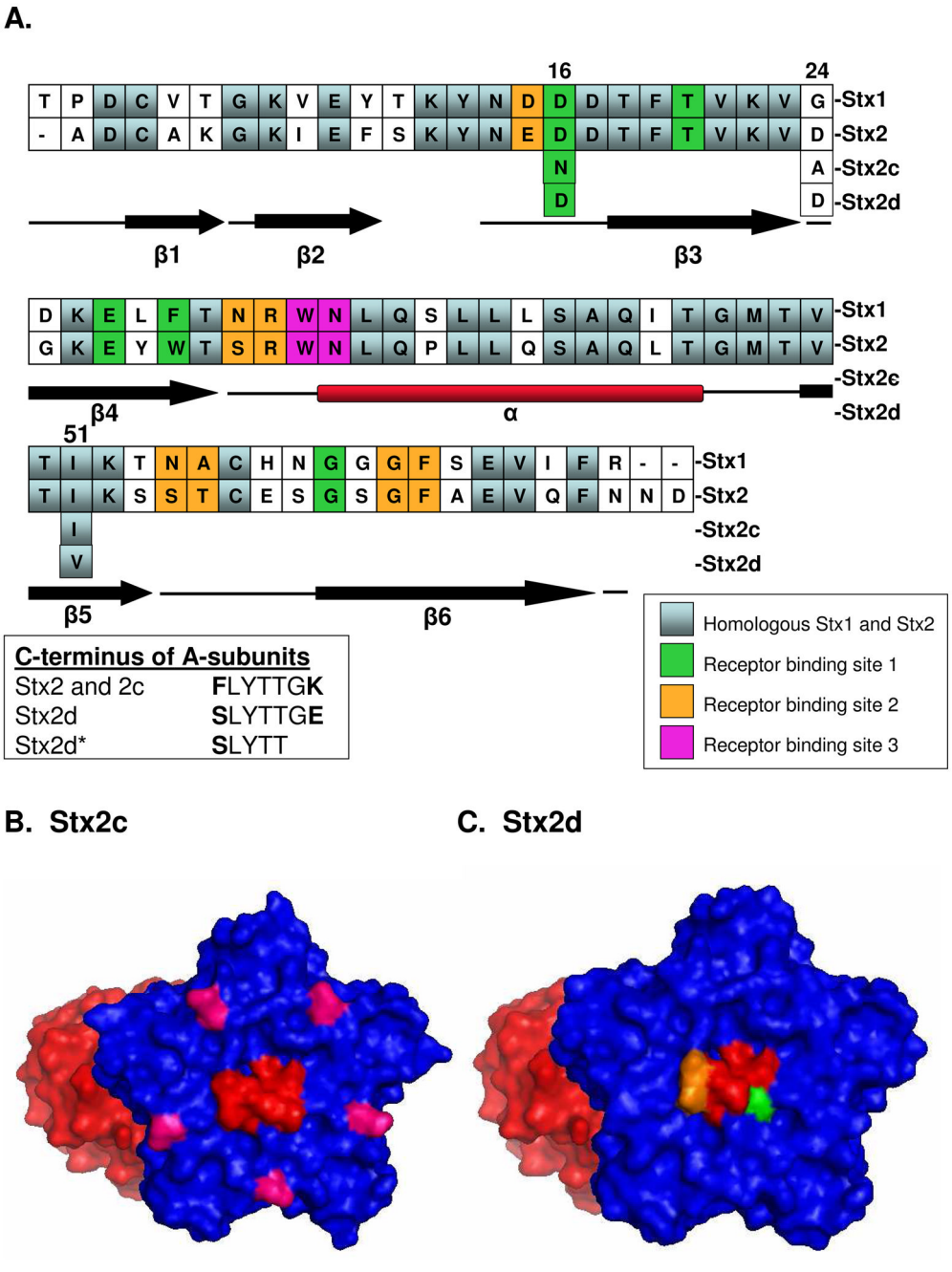

Figure 4. Comparison of the Stx variants

(**A**) The amino acid sequences of the Stx variants. The numbers correspond to the amino acid coordinates of Stx2B; add 1 to obtain the coordinates for Stx1B. Amino acids involved in the receptor binding sites of Stx1 are indicated; similar receptor binding information is not available for Stx2. The C-terminal amino acids of the A-subunit are indicated in the box. **B and C**. Model structures of the Stx2 variants oriented to display the receptor binding sites, generated in PyMol using the published crystal structure of Stx2.(52) The enzymatically active, A subunit is shown in red. The binding or B-subunit, a pentamer of five identical subunits, is shown in blue. (**B**) Stx2c with the amino acid change corresponding to position 16 of the B subunit (D16N) depicted in pink, and the amino acid change D24A could not be

seen in top view since it is located on the opposite side (**C**) Stx2d with the amino acid change corresponding to position 51 of the B subunit (I51V) is not visible since it is buried inside, and the amino acid changes of A subunit corresponding to position 313 (313S) is depicted in green and to position 319 (319E) is depicted in orange.

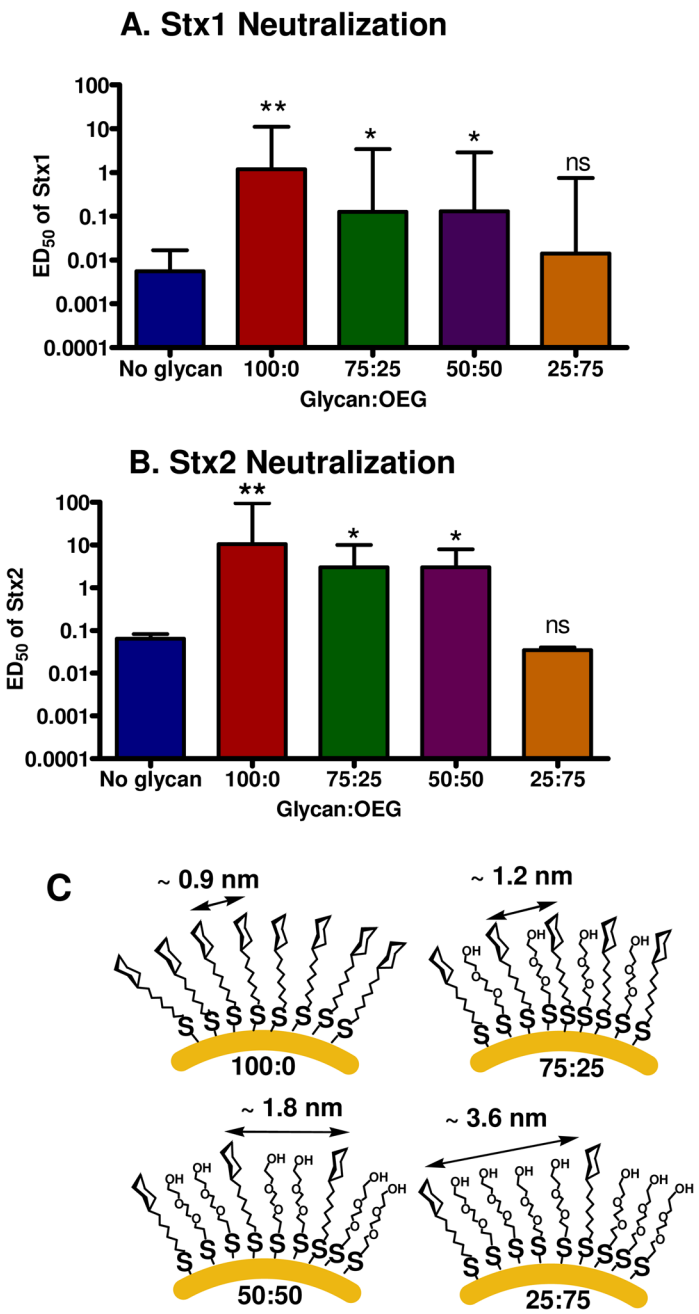

Figure 5.

Effect of varying glycan surface density on inhibition activity (**A**) Stx 1 in presence of GNPs of different glycan surface densities. (**B**) Stx 2 in presence of GNPs of different glycan surface densities. The data are the average ± standard deviation of three experiments. *: P<0.02; **: P<0.002. ns: not significant (**C**) Representation of the gold NP surface with varying density of ligands. Ratio is given as Glycan:OEG.

TABLE 1

Amount of toxin needed to overcome the protective effects of 100 μg/mL of GNPs

	Stx1	Stx2	Stx2c	Stx2d
ED_{50}	**0.07ng/ml**	**0.6ng/ml**	**61ng/ml**	**0.5ng/ml**
ED_{50}+ GNP1 (fold increase)	25.6±17.3[a] (366)	(5)[b]	118±12 (1.9)	1.3±0.5 (2.6)
ED_{50}+ GNP2 (fold increase)	(3)[b]	92 ±8[a] (153)	111±73 (1.8)	19.3±13.9 (39)

[a] Statistically significant compared to control.

[b] Assessed using culture supernatant instead of pure toxin.